# Ferroquadrupole ordering and $\Gamma_5$ rattling motion in the clathrate compound $Ce_3Pd_{20}Ge_6$

Yuichi Nemoto, Takashi Yamaguchi, Takenobu Horino, Mitsuhiro Akatsu, Tatsuya Yanagisawa, and Terutaka Goto
*Graduate School of Science and Technology, Niigata University, Niigata 950-2181, Japan*

Osamu Suzuki
*National Institute for Materials Science, 3-13 Sakura, Tsukuba 305-0003, Japan*

Andreas Dönni
*Department of Physics, Niigata University, Niigata 950-2181, Japan*

Takemi Komatsubara
*Center for Low Temperature Science, Tohoku University, Sendai 980-8578, Japan*

(Received 25 April 2003; revised manuscript received 5 August 2003; published 20 November 2003)

Lattice effects in a cerium based clathrate compound $Ce_3Pd_{20}Ge_6$ with a cubic $Cr_{23}C_6$-type structure have been investigated by ultrasonic and thermal expansion measurements. Elastic softenings of $(C_{11}-C_{12})/2$ and $C_{44}$ proportional to the reciprocal temperature $1/T$ above $T_{Q1}=1.25$ K are well described in terms of the quadrupole susceptibility for the ground state $\Gamma_8$ quartet. A huge softening of 50% in $(C_{11}-C_{12})/2$ and a spontaneous expansion $\Delta L/L=1.9\times10^{-4}$ along the [001] direction in particular indicate the ferroquadrupole ordering of $O_2^0$ below $T_{Q1}$. The elastic anomalies associated with the antiferromagnetic ordering at $T_{N2}=0.75$ K and the incommensurate antiferromagnetic ordering are also found. Notable frequency dependence of $C_{44}$ around 10 K is accounted for by the Debye-type dispersion indicating a $\Gamma_5$ rattling motion of an off-center Ce ion along the [111] direction with eight fractionally occupied positions around the 4a site in a cage. The thermally activated $\Gamma_5$ rattling motion obeying a relaxation time $\tau=\tau_0\exp(E/k_BT)$ with an attempt time $\tau_0=3.1\times10^{-11}$ sec and an activation energy $E=70$ K dies out with decreasing temperature, and then the off-center tunneling state of Ce ion in the 4a-site cage will appear at low temperatures.

DOI: 10.1103/PhysRevB.68.184109 PACS number(s): 62.20.Dc, 71.27.+a, 65.40.De

## I. INTRODUCTION

4f-electronic systems with spin and orbital degrees of freedom in rare earth compounds frequently reveal electric quadrupole orderings in addition to magnetic dipole orderings at low temperatures. The cubic compounds based on $Ce^{3+}$ ion with a $\Gamma_8$ quartet ground state in particular have received much attention because competitive phenomena associated with magnetic dipole, electric quadrupole, and magnetic octupole degrees of freedom are expected. The direct product of $\Gamma_8\otimes\Gamma_8$ is reduced to a direct sum $\Gamma_1\oplus\Gamma_2\oplus\Gamma_3\oplus2\Gamma_4\oplus2\Gamma_5$. The magnetic dipoles $J_x$, $J_y$, and $J_z$ belonging to $\Gamma_4$ symmetry are order parameters for magnetic orderings. The quadrupole orderings of $O_2^0$ and $O_2^2$ with $\Gamma_3$ or $O_{yz}$, $O_{zx}$, and $O_{xy}$ with $\Gamma_5$ are interesting phenomena in the $\Gamma_8$ system. We refer to CeAg exhibiting a ferroquadrupole (FQ) ordering of $O_2^0$ at $T_Q=15$ K.[1,2] $CeB_6$ is known as an antiferroquadrupole ordering of $O_{xy}$ type with the propagation vector of $\boldsymbol{k}=[111]$ at $T_Q=3.2$ K.[3,4] The octupole moments $T_{xyz}$ with $\Gamma_2$ symmetry, $T_x^\alpha$, $T_y^\alpha$, and $T_z^\alpha$ with $\Gamma_4$ and $T_x^\beta$, $T_y^\beta$, and $T_z^\beta$ with $\Gamma_5$, may play a role in the $\Gamma_8$ system.[5]

A cerium-based ternary compound $Ce_3Pd_{20}Ge_6$ with a $\Gamma_8$ ground state has received much attention because the competition between quadrupole and magnetic orderings is expected at low temperatures.[6] $Ce_3Pd_{20}Ge_6$ crystallizes in a cubic $Cr_{23}C_6$-type structure with a space group $Fm\bar{3}m$ consisting of four molecular units with 116 atoms in a unit cell.[7] The 12 Ce sites located in cages are divided into two nonequivalent sites in crystallography. As shown in Fig. 1 the Ce ion, at the 4a site in a cage consisting of 12 Pd atoms and six Ge atoms, possesses a point group symmetry $O_h$, while the Ce ion at the 8c site in a cage of 16 Pd atoms has a symmetry $T_d$. The 4a sites form a face-centered-cubic lattice, while the 8c sites make a simple cubic lattice. Inelastic neutron scattering on $Ce_3Pd_{20}Ge_6$ revealed two overlapping peaks for the crystalline electric field (CEF) potentials, which correspond to magnetic dipole transitions from the $\Gamma_8$ ground quartet to the $\Gamma_7$ excited doublet at 60 K of the 4a site and from the $\Gamma_8$ ground quartet to the $\Gamma_7$ at 46 K of the 8c site.[8] The entropy obtained by low-temperature specific heat measurement on $Ce_3Pd_{20}Ge_6$ also indicates the ground state $\Gamma_8$ quartet at both 4a and 8c sites.[9]

The low-temperature specific heat of $Ce_3Pd_{20}Ge_6$ shows a rounded small peak at $T_{Q1}=1.25$ K and a sharp $\lambda$-peak at $T_{N2}=0.75$ K.[9] Magnetic susceptibility shows a clear cusp at $T_{N2}$, but exhibits no sign of anomaly at $T_{Q1}$.[6] In addition to these experimental results, an elastic softening of $(C_{11}-C_{12})/2$ in our preliminary paper suggests that the paramagnetic phase I transforms to the FQ phase II at $T_{Q1}$ and successively changes to the antiferromagnetic (AFM) phase III at $T_{N2}$.[10] The neutron scattering on $Ce_3Pd_{20}Ge_6$ reveals a paramagnetic state of Ce ions at both 4a and 8c sites even in phase II between $T_{Q1}$ and $T_{N2}$. The AFM ordering in phase III with a propagation vector $\boldsymbol{k}_1=[001]$ for cerium ions at the 4a site is observed below $T_{N2}$.[11] Even in phase III below $T_{N2}$, the 8c site still remains the paramagnetic state. The AFM ordering with incommensurate structure at the 8c site

 

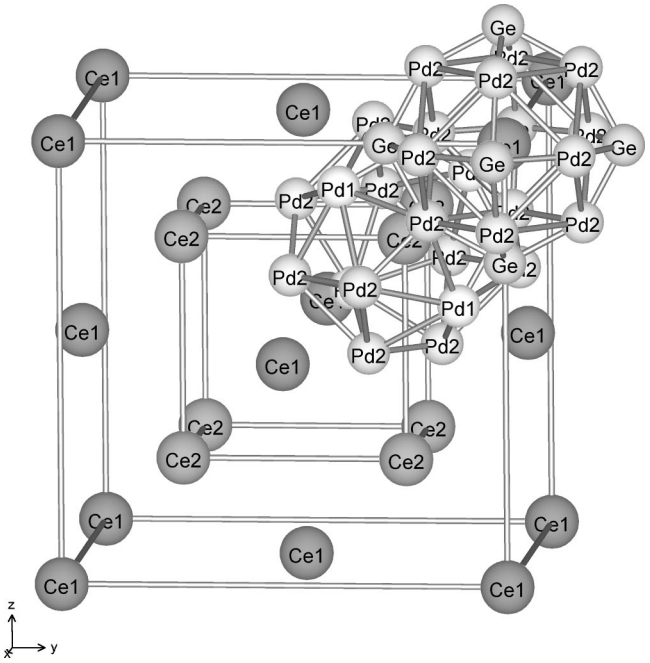


FIG. 1. Cage of the 4a site with $O_h$ symmetry consisting of Ge and the Pd2 atoms and the cage of the 8c site with $T_d$ of Pd1 and Pd2 atoms in the clathrate compound $Ce_3Pd_{20}Ge_6$. The 4a site Ce2 forms a simple cubic lattice, while the 8c site Ce1 makes a face centered cubic one. The ferroquadrupole ordering below $T_{Q1}$ is relevant for the 8c sites and the antiferromagnetic ordering below $T_{N2}$ occurs at the 4a sites. The $\Gamma_5$ rattling motion originates from the off-center Ce1 atom in the 4a-site cage.

appears only below $T_N^* = 0.45$ K.

Clathrate compounds exhibiting rattling motion or off-center motion in a cage have received attention because their remarkable reduction of thermal conductivity is favorable for application to thermoelectric device with a high figure of merit.[12] The ultrasonic waves are scattered by the rattling motion in an oversized cage of a semiconductor $Sr_8Ga_{16}Ge_{30}$ and a filled skutterudite compound $PrOs_4Sb_{12}$.[13,14] The off-center tunneling motion of an OH ion doped in NaCl gives rise to elastic softening at low temperatures.[15] The rattling motion in the present compound $Ce_3Pd_{20}Ge_6$ with a clathrate structure has not been reported so far.

In the present paper we show ultrasonic measurements on $Ce_3Pd_{20}Ge_6$ in order to examine lattice effects associated with the quadrupole ordering and rattling motion in the system. The thermal expansion measurement is also employed to detect the spontaneous distortion below $T_{Q1}$. In Sec. II, the experimental procedure and apparatus are described. The results of the elastic constant, magnetic phase diagram, thermal expansion are presented in Sec. III. The ultrasonic dispersion due to rattling motion is also argued in Sec. III. In Sec. IV, we present concluding remarks.

## II. EXPERIMENT

Single crystals of $Ce_3Pd_{20}Ge_6$ used in the present measurements were grown by a Czochralski puling method. We have made ultrasonic velocity measurements using an apparatus consisting of a phase difference detector. Piezoelectric plates of $LiNbO_3$ for the ultrasonic wave generation and detection are bonded on plane parallel surfaces of sample. The $x$-cut plate of $LiNbO_3$ is available for transverse ultrasonic waves and the 36° $y$-cut plate is for longitudinal waves. The ultrasonic velocity $v$ was measured by fundamental frequencies of 10 MHz and overtone excitations of 30, 50, and 70 MHz. In the estimation of the elastic constant $C = \rho v^2$, we use the mass density $\rho = 10.254$ g/cm$^3$ for $Ce_3Pd_{20}Ge_6$ with a lattice parameter $a = 12.457$ Å.[6]

A homemade $^3$He-refrigerator equipped with a superconducting magnet was used for low-temperature measurements down to 450 mK in magnetic fields up to 12 T. A $^3$He-$^4$He dilution refrigerator with a top-loading probe was used for ultrasonic measurements in the low-temperature region down to 20 mK in fields up to 16 T. The low input-power condition provides low-temperature ultrasonic measurements free from a self-heating effect in the ultrasonic transducers. The sample length as a function of temperature or applied magnetic field was measured precisely by a capacitance dilatometer in the $^3$He refrigerator.

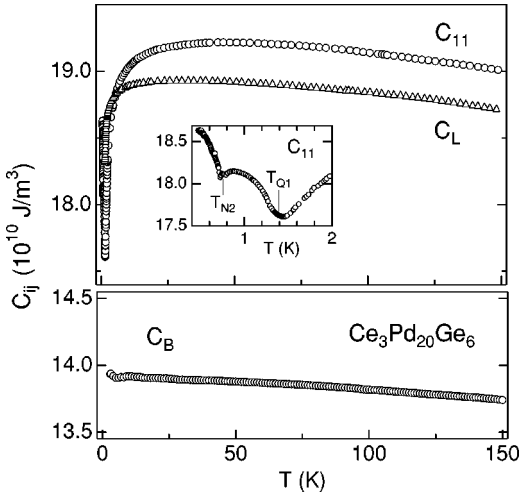


FIG. 2. Temperature dependence of the elastic constants $C_{11}$ and $C_L$ and the bulk modulus $C_B$ of $Ce_3Pd_{20}Ge_6$. The inset shows the anomalies of $C_{11}$ around the ferroquadrupole transition $T_{Q1} = 1.25$ K and the antiferromagnetic transition $T_{N2} = 0.75$ K.

## III. RESULTS AND DISCUSSIONS

### A. Temperature dependence of the elastic constants

The elastic constants of $C_{11}$ and $C_L = (C_{11} + C_{12} + 2C_{44})/2$ of $Ce_3Pd_{20}Ge_6$ in Fig. 2 were measured by longitudinal ultrasonic waves with frequencies 10 MHz propagating along the [100] and [110] directions, respectively. The elastic constant $(C_{11} - C_{12})/2$ of $Ce_3Pd_{20}Ge_6$ in Fig. 3 was measured by a transverse ultrasonic wave of 10 MHz propagating along the [110] direction polarized to the $[1\bar{1}0]$ one. The elastic constant $C_{44}$ of $Ce_3Pd_{20}Ge_6$ in Fig. 3 was determined by a transverse wave of 30 MHz propagating along [100] polarized to [010]. The bulk modulus $C_B = (C_{11} + 2C_{12})/3$ in Fig. 2 was calculated by $C_{11}$ in Fig. 2 and $(C_{11} - C_{12})/2$ in Fig. 3.

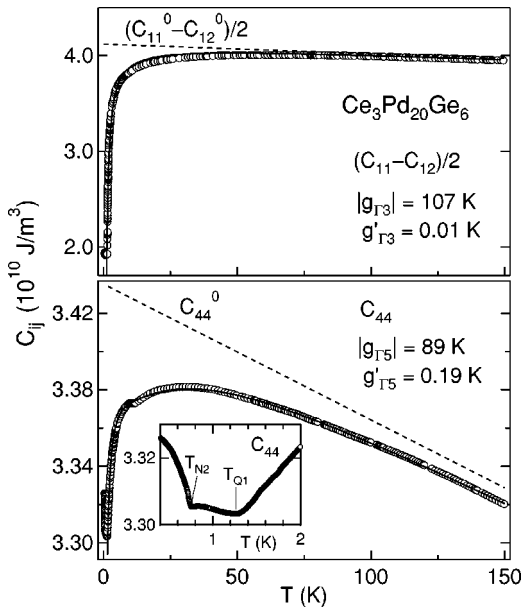


FIG. 3. Temperature dependence of the elastic constants $(C_{11}-C_{12})/2$ and $C_{44}$ corresponding to shear waves in $Ce_3Pd_{20}Ge_6$. The inset shows the anomalies of $C_{44}$ around the ferroquadrupole transition $T_{Q1}=1.25$ K and the antiferromagnetic transition $T_{N2}=0.75$ K. Solid lines are the calculation by the quadrupole susceptibility for the $\Gamma_8$ ground state and the $\Gamma_7$ state at 46 K of Ce ions. The broken lines are background $C_\Gamma^0$, as shown in the text. A shoulder in $C_{44}$ around 30 K means an ultrasonic dispersion due to the $\Gamma_5$ rattling motion.

It is remarkable that $(C_{11}-C_{12})/2$ exhibits a huge softening of 50% with decreasing temperature down to $T_{Q1}=1.25$ K. In phase II below $T_{Q1}$ the ultrasonic echo signal of the $(C_{11}-C_{12})/2$ mode completely disappears due to a marked ultrasonic attenuation. The softening of the longitudinal $C_{11}$ and $C_L$ modes in Fig. 2 originates from the softening of $(C_{11}-C_{12})/2$, because $C_{11}$ and $C_L$ involve $(C_{11}-C_{12})/2$ in part. The softening of $(C_{11}-C_{12})/2$ above $T_{Q1}$ and the spontaneous tetragonal distortion below $T_{Q1}$, that will be shown in Sec. III D, provide evidence for the FQ ordering in phase II. $C_{44}$ in Fig. 3 also exhibits a softening of 2.5% down to $T_{Q1}$. The low-temperature behavior of $C_{11}$ and $C_{44}$ shown in insets of Figs. 2 and 3 indicates the transition to the FQ phase II at $T_{Q1}$ and successive transition to the AFM phase III at $T_{N2}=0.75$ K. On the other hand, $C_B$ shows a monotonic increase with decreasing temperature.

Neutron scattering on $Ce_3Pd_{20}Ge_6$ revealed paramagnetic state for Ce ions at both 4a and the 8c sites in phase II, which is consistent with the present scenario of the FQ ordering at 8c site in phase II below $T_{Q1}$.[11] AFM ordering in phase III at the 4a site below $T_{N2}$ has been detected by neutron scattering. It has been proposed that the intersite quadrupole interaction among 8c sites brings about the FQ ordering at 8c sites in phase II and Ce ions at 4a sites still remain in a parastate even in phase II. The intersite magnetic interaction among 4a sites gives rise to the AFM ordering in phase III below $T_{N2}$. The magnetic ordering at 8c sites appears only below 0.4 K. We discuss this transition in Sec. III C.

### B. Quadrupole susceptibility

In order to analyze the elastic softening of $(C_{11}-C_{12})/2$ and $C_{44}$ in $Ce_3Pd_{20}Ge_6$ of Fig. 3, we introduce the coupling of the quadrupole $O_{\Gamma\gamma}$ of Ce ions to the elastic strain $\varepsilon_{\Gamma\gamma}$ as[16]

$$H_{QS}=-\sum_i g_\Gamma O_{\Gamma\gamma}(i)\varepsilon_{\Gamma\gamma}, \tag{1}$$

where the summation $\Sigma_i$ takes over Ce ions in unit volume, and $g_\Gamma$ is a coupling constant. The intersite quadrupole interaction mediated by phonons and conduction electrons is written in a mean field approximation as

$$H_{QQ}=-\sum_j g'_\Gamma\langle O_{\Gamma\gamma}\rangle O_{\Gamma\gamma}(j), \tag{2}$$

where $\langle O_{\Gamma\gamma}\rangle$ denotes a mean field of the quadrupole and $g'_\Gamma$ means a coupling constant for the intersite quadrupole interaction. By differentiating the total free energy consisting of 4f-electron and lattice parts with respect to the elastic strain $\varepsilon_{\Gamma\gamma}$, we obtain the temperature dependence of the elastic constant $C_\Gamma(T)$ as[16]

$$C_\Gamma(T)=C_\Gamma^0-\frac{Ng_\Gamma^2\chi_\Gamma(T)}{1-g'_\Gamma\chi_\Gamma(T)}. \tag{3}$$

Here $C_\Gamma^0(T)$ denotes a background elastic constant without the quadrupole-strain interaction and $N$ is the number of Ce ions in unit volume. The quadrupole susceptibility of $\chi_\Gamma(T)$ in Eq. (3) is written as

$$-g_\Gamma^2\chi_\Gamma(T)=\left\langle\frac{\partial^2E_i}{\partial\varepsilon_{\Gamma\gamma}^2}\right\rangle-\frac{1}{k_BT}\left\{\left\langle\left(\frac{\partial E_i}{\partial\varepsilon_{\Gamma\gamma}}\right)^2\right\rangle-\left\langle\frac{\partial E_i}{\partial\varepsilon_{\Gamma\gamma}}\right\rangle^2\right\}, \tag{4}$$

where $E_i$ is a second-order perturbation energy with respect to $\varepsilon_{\Gamma\gamma}$ for the CEF state.[16] The first part on the right-hand side of Eq. (4) corresponds to the Van Vleck term and the second part to the Curie term. The Ce ions at both 4a and 8c sites in $Ce_3Pd_{20}Ge_6$ have a $\Gamma_8$ ground state, while the $\Gamma_7$ state has excited energies of 46 K at the 8c site and 60 K at the 4a site. As already mentioned, the neutron scattering revealed that the FQ ordering of 8c sites occurs at $T_{Q1}=1.25$ K and the AFM ordering of 4a sites appears at $T_{N2}=0.75$ K. These facts indicate that the intersite quadrupole interaction of Eq. (2) among the Ce ions at 8c sites dominates the softening of $(C_{11}-C_{12})/2$ as a precursor of the FQ ordering at $T_{Q1}$. In the following analysis we simply assume a quadrupole-strain interaction of Eq. (1) and a quadrupole interaction of Eq. (2) for the 8c site with the CEF splitting of $\Gamma_8$ (0 K) and $\Gamma_7$ (46 K).

The solid lines for $(C_{11}-C_{12})/2$ and $C_{44}$ with Eq. (3) in Fig. 3 reproduce well the softening in the paramagnetic phase I above $T_{Q1}$. It should be noted that the softening above $T_{Q1}$, proportional to the reciprocal temperature $1/T$, originates from the Curie term of Eq. (4). The coupling constants were determined to be $|g_{\Gamma 3}|=107$ K, $g'_{\Gamma 3}=0.01$ K for $(C_{11}-C_{12})/2$, and $|g_{\Gamma 5}|=89$ K, $g'_{\Gamma 5}=0.19$ K for $C_{44}$. The

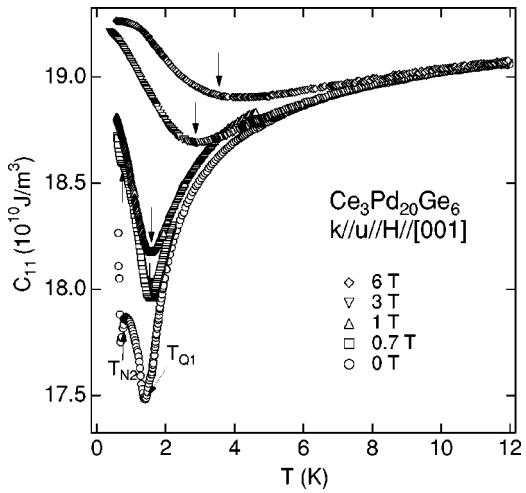


FIG. 4. Low-temperature behavior of $C_{11}$ of $Ce_3Pd_{20}Ge_6$ under magnetic fields along the [001] direction. Downward arrows indicate the ferroquadrupole ordering temperature $T_{Q1}$, and the upward arrow means the antiferromagnetic ordering temperature $T_{N2}$.

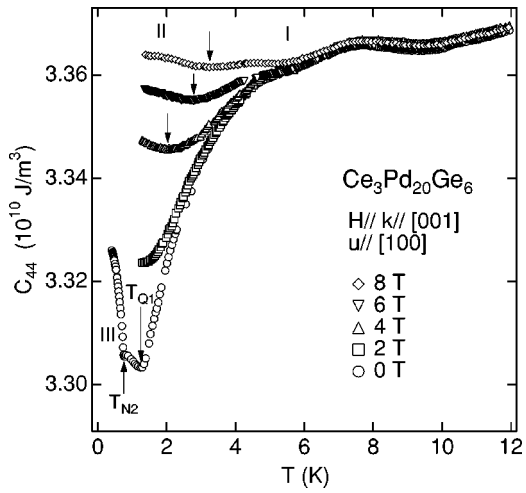


FIG. 5. Low-temperature behavior of $C_{44}$ of $Ce_3Pd_{20}Ge_6$ under magnetic fields along [001]. Downward arrows indicate the ferroquadrupole ordering temperature $T_{Q1}$, and the upward arrow means the antiferromagnetic ordering temperature $T_{N2}$.

background $(C_{11}^0 - C_{12}^0)/2 = (4.12 - 0.001T) \times 10^{10}$ J/m$^3$ and $C_{44}^0 = (3.44 - 0.0007T) \times 10^{10}$ J/m$^3$ indicated by broken lines in Fig. 3 was used. The positive value of $g'_{\Gamma 3} > 0$ are consistent with the FQ ordering in $Ce_3Pd_{20}Ge_6$. A shoulderlike anomaly in $C_{44}$ around 10 K results from ultrasonic dispersion that is caused by a rattling motion of the rare-earth ion at the 4a site in an oversized cage of Fig. 1. We discuss this remarkable behavior in Sec. III E.

### C. Magnetic phase diagram

In order to examine the magnetic phase diagrams of the FQ and AFM orderings in $Ce_3Pd_{20}Ge_6$, we have made low-temperature ultrasonic measurements of $C_{11}$, $C_{44}$ and $(C_{11} - C_{12})/2$ under magnetic fields. The softening of $C_{11}$ of Fig. 4 reduces with increasing fields applied along the [001] direction parallel to the propagation direction of longitudinal wave. The FQ transition points $T_{Q1}$, indicated by downward arrows in Fig. 4, shift to higher temperatures and become indistinct in high fields up to 6 T. In Fig. 5, the FQ transition points $T_{Q1}$ also shift to higher temperatures, accompanied by a reduction of the softening in $C_{44}$ with increasing applied fields along the [001] direction.

In Figs. 6 and 7, we show the field dependence of $(C_{11} - C_{12})/2$ applying fields along the [001] and [110] directions, respectively. In a zero magnetic field, the $(C_{11} - C_{12})/2$ mode exhibits a considerable softening of 50% and a strong ultrasonic attenuation, losing the echo signal in the vicinity of the FQ transition $T_{Q1} = 1.25$ K. The magnitude of the softening decreases abruptly with increasing fields along both [001] and [110] directions. In magnetic fields, clear minima of $(C_{11} - C_{12})/2$ corresponding to the transitions $T_{Q1}$ from the paramagnetic phase I to the FQ phase II shift to higher temperatures. Only broad round anomalies around $T_{Q1}$ have been observed in high fields of 5 T. This behavior of $T_{Q1}$ is similar to the results of the FQ ordering accompanied by the soft $C_{44}$ mode in $HoB_6$.[17] The Neel temperature $T_{N2}$ in Fig. 6 shifts slightly to lower temperatures with increasing magnetic fields. In Fig. 7 the anomalies associated with the transition between phase II and II′ below $T_{Q1}$ have been found.

For the investigation of low-temperature and high-field behavior in FQ II and AFM III phases, we have measured field dependence of the $C_{44}$ and $C_L = (C_{11} + C_{12} + 2C_{44})/2$ employing the dilution refrigerator. In Fig. 8 we show $C_{44}$ versus $H$ at 30 mK in fields up to 12 T applied along [001]. The inset of Fig. 8 is an expanded view below 2.5 T. An anomaly of the phase II-III boundary at 2.1 T indicated by a vertical line has been observed. Furthermore, several anomalies at 0.5, 1.2, and 1.6 T associated with subphases of phase III have been found. It should be emphasized that appreciable hysteresis phenomena between increasing and decreasing field sequences have been found only in phase III.

In Fig. 9 we show the low-temperature field dependence of the $C_L$ in fields up to 16 T applied along [110]. The

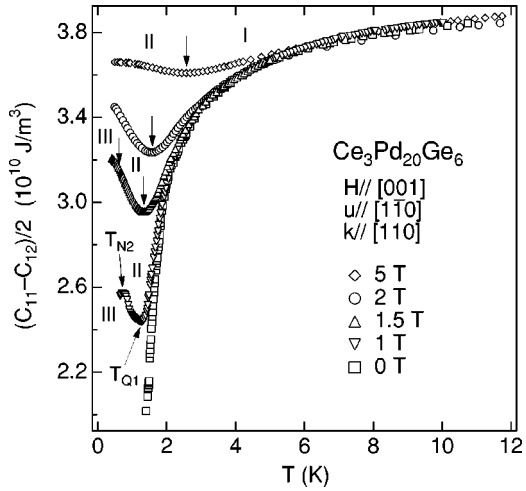


FIG. 6. Low temperature behavior of $(C_{11} - C_{12})/2$ of $Ce_3Pd_{20}Ge_6$ under magnetic fields along the [001] direction. The successive phase transitions I-II-III are indicated by arrows.

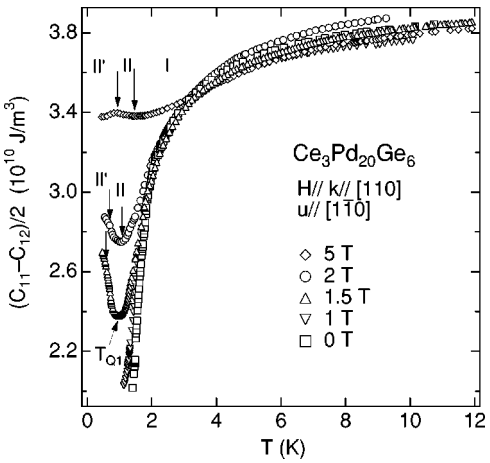


FIG. 7. Low temperature behavior of $(C_{11}-C_{12})/2$ of $Ce_3Pd_{20}Ge_6$ under magnetic fields along the [110] direction. The successive phase transitions I-II-II′ are indicated by arrows.

low-field behavior below 2.5 T is shown in the inset of Fig. 9. We have observed a new phase boundary around 8.2 T in phase II, which is probably a subphase of the FQ phase II. However, this phase boundary is absent in fields along [001] as shown in Fig. 8. At low field in phase III, we have found several anomalies in $C_L$ of Fig. 9 showing a hysteresis behavior. As can been seen in the inset of Fig. 9, this hysteresis becomes pronounced with decreasing temperature. These subphases with hysteresis behavior in phase III in magnetic fields along both [001] and [110] are very consistent with the results of neutron scattering experiments that detect weak incommensurate magnetic Bragg peaks with a propagation vector $\boldsymbol{k}=[0\ 0\ 1-\tau]$, ($\tau\sim0.06$) at the 8c site.[11]

The magnetic phase diagrams of $Ce_3Pd_{20}Ge_6$ in Figs. 10 and 11 are obtained in fields along the [001] and [110] directions, respectively. We present the results of the ultrasonic measurements together with the results of thermal expansions in Sec. III D. It is of importance that the FQ phase II is stabilized in fields for the [001] direction in Fig. 10 and the

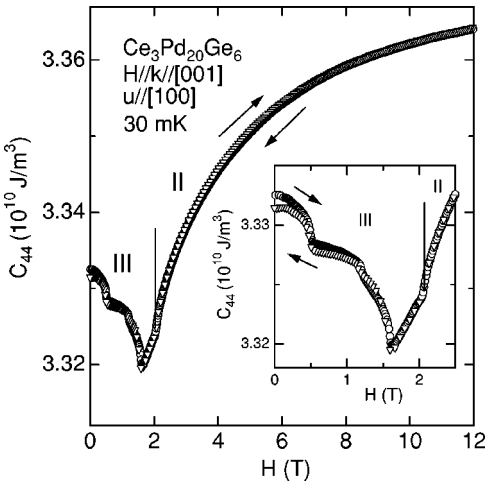


FIG. 8. Field dependence of $C_{44}$ at 30 mK in fields along [001] up to 12 T. The inset is an expanded view below 2.5 T indicating the magnetic transitions.

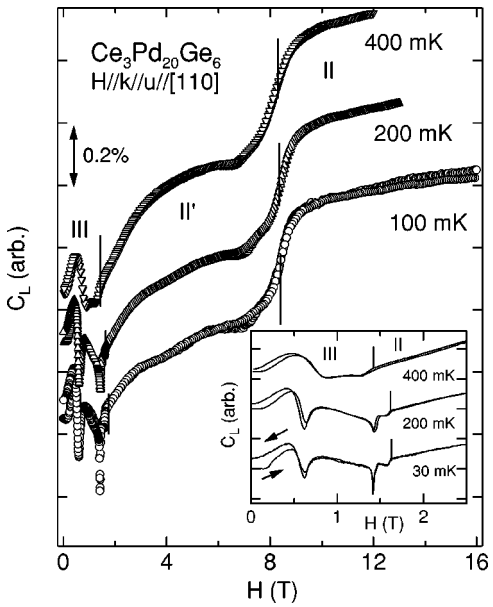


FIG. 9. Field dependence of the $C_L=(C_{11}+C_{12}+2C_{44})/2$ at various temperatures in fields along [110] up to 16 T. The inset is an expanded view below 2.5 T indicating the magnetic transitions.

[110] direction in Fig. 11. The FQ subphase II′ was added to the phase diagram and the upper limit at 8.2 T of the phase II′ newly determined in fields along [110] of Fig. 11. However, the FQ subphase is absent in fields along [001] of Fig. 10. This result indicates strong anisotropy of the quadrupole interaction of $O_2^0$ in $Ce_3Pd_{20}Ge_6$.

The series of $R_3Pd_{20}X_6$ compounds usually show two successive AFM orderings of the 8c site at $T_{N1}$ with a propagation vector $\boldsymbol{k}_1=[111]$ and of the 4a site at $T_{N2}(<T_{N1})$ with $\boldsymbol{k}_2=[001]$, $Nd_3Pd_{20}Ge_6$ ($T_{N1}=1.75$ K, $T_{N2}=0.58$ K),[18] $Nd_3Pd_{20}Si_6$ ($T_{N1}=2.4$ K, $T_{N2}=0.7$ K),[19] $Tb_3Pd_{20}Si_6$ ($T_{N1}=10.2$ K, $T_{N2}=4.1$ K),[20] $Dy_3Pd_{20}Si_6$ ($T_{N1}\sim5.8$ K, $T_{N2}$

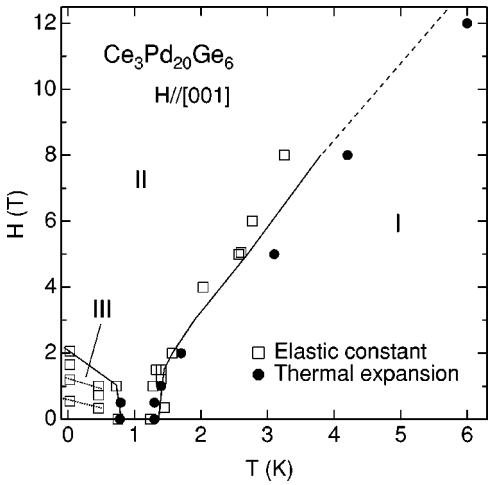


FIG. 10. Magnetic phase diagram of $Ce_3Pd_{20}Ge_6$ under fields along the [001] direction. The boundary from paramagnetic phase I to the ferroquadrupole phase II shifts to higher temperatures with increasing fields, while the boundary from phase II to the antiferromagnetic phase III shifts to lower temperatures in fields.

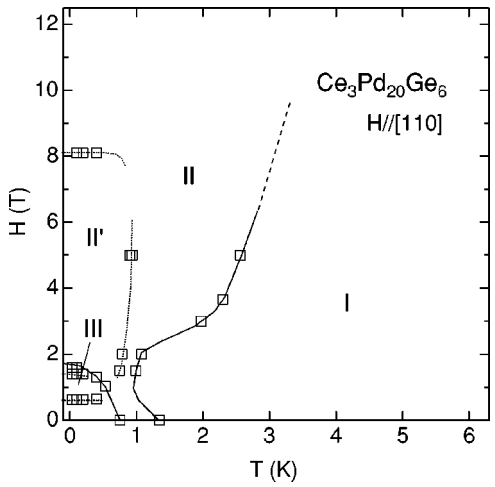


FIG. 11. Magnetic phase diagram of $Ce_3Pd_{20}Ge_6$ under fields along the [110] direction. The subphase II′ exists in the AFQ phase II.

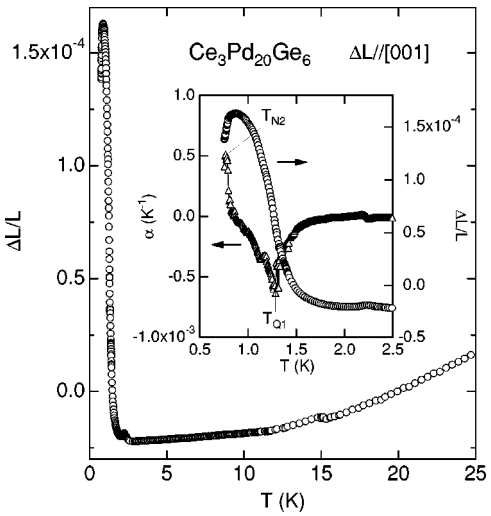


FIG. 12. Thermal expansion $\Delta L/L$ in $Ce_3Pd_{20}Ge_6$. The inset shows the thermal expansion coefficient $\alpha$ and thermal expansion $\Delta L/L$ at low temperatures.

$\sim 1.8$ K),[21] and so on. One can reasonably expect that the transition temperature $T_{N1}$ at the 8c site is always higher than $T_{N2}$ at the 4a site since the distance $\sim 6.2$ Å between rare-earth ion of the 8c site is much shorter than the one $\sim 8.8$ Å of the 4a site. In the present $Ce_3Pd_{20}Ge_6$, at first the FQ ordering at the 8c site with a structural change from a cubic lattice to a tetragonal one occurs at $T_{Q1}=1.25$ K. Therefore, the AFM ordering at the 8c site takes place with difficulty because the favorable propagation vector $\boldsymbol{k}_1=[111]$ of the 8c site does not match the tetragonal lattice in phase II. In other words, the AFM ordering at the 8c site is replaced by the FQ ordering in $Ce_3Pd_{20}Ge_6$. However, the AFM ordering of the 4a site with a propagation vector $\boldsymbol{k}_2=[001]$ occurs easily even in a tetragonal structure below $T_{N2}$. Neutron experiments detected a large enough value of saturation cerium moment $\mu(4a)=(1.1\pm 0.1)\mu_B$/Ce that is expected from the ground state quartet $\Gamma_8$ perpendicular to the $\boldsymbol{k}_1=[001]$ in $Ce_3Pd_{20}Ge_6$ far below $T_{N2}$ at 50 mK.[11]

### D. Thermal expansion

In order to examine the structural change due to the FQ ordering at $T_{Q1}=1.25$ K, we have measured the thermal expansion along the [001] direction in $Ce_3Pd_{20}Ge_6$. The sample lengths along the [001] and [111] directions are written by the symmetry strains as $(\Delta L/L)_{[001]}=\varepsilon_{zz}=\varepsilon_B/3+\varepsilon_u/\sqrt{3}$ and $(\Delta L/L)_{[111]}=\varepsilon_B/3+2(\varepsilon_{yz}+\varepsilon_{zx}+\varepsilon_{xy})/3$. Here, $\varepsilon_B=\varepsilon_{xx}+\varepsilon_{yy}+\varepsilon_{zz}$ is a volume strain with $\Gamma_1$ symmetry, $\varepsilon_u=(2\varepsilon_{zz}-\varepsilon_{xx}-\varepsilon_{yy})/\sqrt{3}$ is a tetragonal strain with $\Gamma_3$, and $\varepsilon_{xy}$ is a shear strain with $\Gamma_5$. The length along [001] in Fig. 12 shows a monotonic decrease with decreasing temperature in the paramagnetic phase I above $T_{Q1}$ and abruptly expands about $\Delta L/L=1.9\times 10^{-4}$ below $T_{Q1}$. The thermal expansion along [001] in phase II and the huge softening of 50% in $(C_{11}-C_{12})/2$ of Fig. 3 indicate the $O_2^0$-type FQ ordering accompanied by the structural transition from cubic lattice to tetragonal one with the spontaneous strain $\langle\varepsilon_u\rangle$ in phase II. This spontaneous strain is proportional to the order parameter as $\langle\varepsilon_u\rangle=Ng_{\Gamma 3}\langle O_2^0\rangle[2/(C_{11}^0-C_{12}^0)]$ in the mean-field approximation. Below $T_{N2}=0.75$ K, the $\Delta L/L$ along [001] slightly shrinks. The inset of Fig. 12 is an expanded view of $\Delta L/L$ and the coefficient of the thermal expansion $\alpha$ at low temperatures. A sharp anomaly in the coefficient $\alpha$ has been found at the FQ transition $T_{Q1}$.

Measurements of $\Delta L/L$ versus $T$ in various magnetic fields parallel to [001] are shown in Fig. 13. The magnitude of the expansion $\Delta L/L$ in fields exhibits a noticeable increase up to $\Delta L/L=2.5\times 10^{-4}$ compared with that in zero magnetic field. The sharp increase of $\Delta L/L$ at the transition point to the FQ phase II has been observed in low magnetic fields below 1 T. On the other hand, the gradual increase in the thermal expansion $\Delta L/L$ above 5 T up to 12 T indicates an obscure character of the I-II phase boundary in high fields. This is consistent with the fact that the elastic constants in fields of Figs. 4, 5, 6, and 7 show obscure transi-

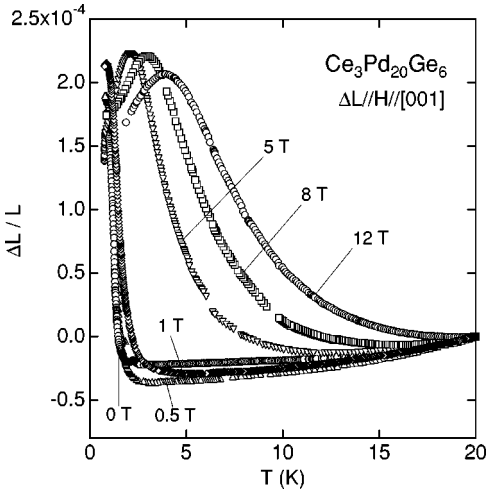


FIG. 13. Thermal expansion $\Delta L/L$ along [001] in $Ce_3Pd_{20}Ge_6$ under fields up to 12 T along the [001] direction.

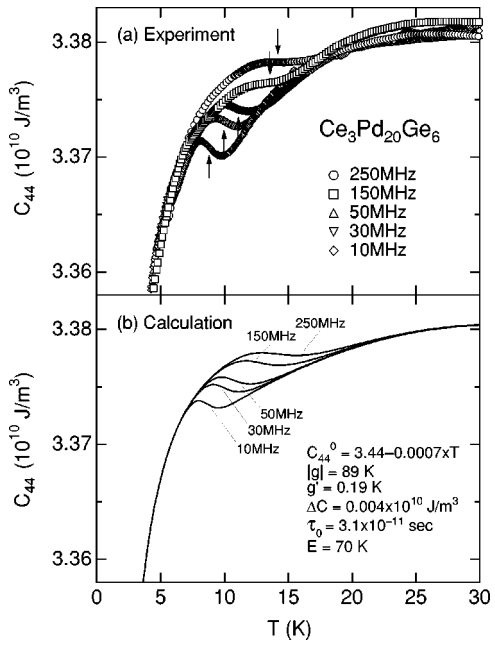


FIG. 14. Frequency dependence of the elastic constant of the transverse $C_{44}$ mode in $Ce_3Pd_{20}Ge_6$. (a) represents the experimental results with the frequencies from 10 MHz up to 250 MHz. (b) is the calculation in terms of the Debye-type dispersion of Eq. (5) in the text.

tions in fields. This behavior is similar to the liquid-gas transition near the critical end point under hydrostatic pressures.

The thermal expansion along the [001] direction in fields parallel to [001] and the considerable softening of $(C_{11}-C_{12})/2$ of 50% in $Ce_3Pd_{20}Ge_6$ strongly suggests that the order parameter of the FQ ordering in phase II is $O_2^0$, with a $\Gamma_3$ symmetry. The relatively small softening of 2.5% in $C_{44}$ in Fig. 3 means that the quadrupole of $O_{xy}$-type with $\Gamma_5$ is irrelevant for the transition at $T_{Q1}$. The thermal expansion of $Ce_3Pd_{20}Ge_6$ along [111] is required to examine an interplay of the spontaneous strain $\varepsilon_{xy}$ for the phase II. We refer to our recent study of the FQ transition in $HoB_6$ and the phase IV in $Ce_xLa_{1-x}B_6$ ($x=0.75$ and 0.70),[17,22] where the trigonal strain $\varepsilon_{yz}=\varepsilon_{zx}=\varepsilon_{xy}$ plays a significant role and the tetragonal strain $\varepsilon_u$ is irrelevant. These facts are very consistent with the pronounced elastic softening in $C_{44}$ of 70% in $HoB_6$ and of 31% in $Ce_xLa_{1-x}B_6$ ($x=0.75$ and 0.70).

### E. Ultrasonic dispersion of $C_{44}$

The $C_{44}$ mode associated with the elastic strain $\varepsilon_{yz}$, $\varepsilon_{zx}$, and $\varepsilon_{xy}$ of $\Gamma_5$ symmetry of $Ce_3Pd_{20}Ge_6$ in Figs. 3 and 5 exhibits a shoulderlike anomaly around 10 K in addition to the characteristic softening due to the quadrupolar coupling above $T_{Q1}=1.25$ K. It should be noted that this anomaly is absent for the $(C_{11}-C_{12})/2$ mode associated with $\Gamma_3$ elastic strain $\varepsilon_v$ and the bulk modulus $C_B$ with $\Gamma_1$ volume strain $\varepsilon_B$. In order to examine the origin of this anomaly, we have measured the frequency dependence of $C_{44}$ from 10 to 250 MHz. The elastic constant $C_{44}$ of Fig. 14(a) exhibits shoulders showing a remarkable frequency dependence. An increase in the ultrasonic attenuation around the shoulder has also been found, but is not discussed here. We describe this frequency dependence of the elastic constant $C_{44}^D(\omega)$ in terms of Debye-type dispersion as

$$C_{44}^D(\omega)=C_{44}^D(\infty)-\frac{C_{44}^D(\infty)-C_{44}^D(0)}{1+\omega^2\tau^2}, \tag{5}$$

where $C_{44}^D(\infty)$ and $C_{44}^D(0)$ are the elastic constants of the high frequency limit and the low frequency one, respectively. Here $\omega$ is an angular frequency of the ultrasonic wave and $\tau$ means the relaxation time of the system. In fittings of Fig. 14(b), we take into account the superposition of two susceptibilities by the quadrupole one of Eq. (3) and the Debye-type dispersion of Eq. (5) as $C_{44}=C_{44}^Q+C_{44}^D(\omega)$. The inflection points around 10 K in $C_{44}$, indicated by arrows in Fig. 14(a) show the temperatures where $\tau$ coincides with $\omega$ as $\omega\tau=1$. The ultrasonic attenuation is expected to be maximum at the temperatures for $\omega\tau=1$. The solid lines of Fig. 14(b), being calculations made with Eq. (5), well reproduce the experimental results of Fig. 14(a). The relaxation time obeying the Arrhenius-type temperature dependence $\tau=\tau_0\exp(E/k_BT)$ with the attempt time $\tau_0=3.1\times10^{-11}$ sec and the activation energy $E=70$ K has been determined. The parameter of $\Delta C=C_{44}^D(\infty)-C_{44}^D(0)=0.004\times10^{10}$ J/m$^3$ is used.

The ultrasonic dispersion due to electron thermal hopping has already found in the inhomogeneous valence fluctuation compounds of $Sm_3X_4$ ($X=$Se, Te), $Yb_4(As_{0.71}Sb_{0.29})_3$ (Ref. 23) and $Sr_{12}Ca_2Cu_{24}O_{41}$[24]. It is remarkable that the very slow relaxation time $\tau$ and extremely low activation energy $E$ for $Ce_3Pd_{20}Ge_6$ are exceptional as compared to those of charge fluctuation compounds $Sm_3Se_4$ (Ref. 25) and $Sm_3Te_4$,[26] $\tau_0\sim2.5\times10^{-13}$ sec and $E\sim1600$ K, and $Sr_{12}Ca_2Cu_{24}O_{41}$, $\tau_0=1.01\times10^{-13}$ sec and $E=1900$ K.[24] This discrepancy, of the order of $\tau_0$ and $E$ between the present $Ce_3Pd_{20}Ge_6$ and the charge fluctuation compounds, indicates that a thermally activated rattling motion of the heavy mass particle, which is probably a rare-earth ion in a cage, gives rise to the ultrasonic dispersion in $Ce_3Pd_{20}Ge_6$.

Glass materials and charge fluctuation compounds exhibit frequently the ultrasonic dispersion, which results from a thermally activated motion in a double-well or multiwell potential. The compounds such as $Sm_3X_4$ ($X=$S, Se, Te) with different valence of $Sm^{2+}$ and $Sm^{3+}$ ions and $Sr_{12}Ca_2Cu_{24}O_{41}$ with $Cu^{2+}$ and $Cu^{3+}$ ions cause the ultrasonic dispersions due to thermally assisted charge fluctuation in the temperature region between 100 and 200 K. The two-level system (TLS) due to an atomic tunneling[27] or electron tunneling[26] manifests itself in glass materials at low temperatures, where the thermally activated motion dies out. The TLS yields the decrease in the elastic constant proportional to $\ln T$,[28] the specific heat to $T$, and the thermal conductivity to $T^2$.[29] In the case of $Sm_3Te_4$, a remarkable logarithmic decrease in the elastic constant appears below about 15 K down to the spin glass transition at $T_g=1.5$ K, which suggests the existence of a 4f-electron tunneling motion between $Sm^{2+}$ and $Sm^{3+}$ ions situated at the charge glass state.[26]

TABLE I. Rattling modes with eight off-center positions along the threefold [111] direction in the 4a-site cage with $O_h$ point group symmetry. Corresponding elastic strains are also listed. There is a $\Gamma_5$ rattling mode coupled to the $\varepsilon_{xy}$-type strain of the $C_{44}$ mode. This is contrary to the absence of the $\Gamma_3$ rattling mode to the $\varepsilon_u, \varepsilon_v$ of the $(C_{11}-C_{12})/2$ mode. The present ultrasonic dispersion in $C_{44}$ of $Ce_3Pd_{20}Ge_6$ originates from the $\Gamma_5$-type rattling at the 4a site.

| Symmetry | Rattling mode | Strain |
|---|---|---|
| $\Gamma_1$ | $\rho_{\Gamma 1}=\rho_1+\rho_2+\rho_3+\rho_4+\rho_5+\rho_6+\rho_7+\rho_8$ | $\varepsilon_B=\varepsilon_{xx}+\varepsilon_{yy}+\varepsilon_{zz}$ |
| $\Gamma_2$ | $\rho_{\Gamma 2}=\rho_1+\rho_2+\rho_3+\rho_4-\rho_5-\rho_6-\rho_7-\rho_8$ | |
| $\Gamma_3$ | | $\varepsilon_u=(2\varepsilon_{zz}-\varepsilon_{xx}-\varepsilon_{yy})/\sqrt{3}$ |
| | | $\varepsilon_v=\varepsilon_{xx}-\varepsilon_{yy}$ |
| $\Gamma_4$ | $\rho_{\Gamma 4,x}=\rho_1-\rho_2-\rho_3+\rho_4+\rho_5-\rho_6+\rho_7-\rho_8$ | |
| | $\rho_{\Gamma 4,y}=\rho_1-\rho_2+\rho_3-\rho_4+\rho_5-\rho_6-\rho_7+\rho_8$ | |
| | $\rho_{\Gamma_4,z}=\rho_1+\rho_2-\rho_3-\rho_4-\rho_5-\rho_6+\rho_7+\rho_8$ | |
| $\Gamma_5$ | $\rho_{\Gamma_5,yz}=\rho_1-\rho_2-\rho_3+\rho_4-\rho_5+\rho_6-\rho_7+\rho_8$ | $\varepsilon_{yz}$ |
| | $\rho_{\Gamma_5,zx}=\rho_1-\rho_2+\rho_3-\rho_4-\rho_5+\rho_6+\rho_7-\rho_8$ | $\varepsilon_{zx}$ |
| | $\rho_{\Gamma_5,xy}=\rho_1+\rho_2-\rho_3-\rho_4+\rho_5+\rho_6-\rho_7-\rho_8$ | $\varepsilon_{xy}$ |

The present clathrate compound $Ce_3Pd_{20}Ge_6$ is a crystal possessing an ideal periodic arrangement of cages in space. The stable trivalent Ce ions in cages of $Ce_3Pd_{20}Ge_6$ are free from the valence fluctuation phenomena. As shown in Fig. 1, the clathrate compound $Ce_3Pd_{20}Ge_6$ is made up of a cage at the 4a site consisting of Pd and Ge with distances $d_{\text{Ce1-Ge}}=3.332$ Å and $d_{\text{Ce1-Pd2}}=3.067$ Å, and the cage at the 8c site of Pd with $d_{\text{Ce2-Pd1}}=2.868$ Å and $d_{\text{Ce2-Pd2}}=3.373$ Å. The trivalent Ce ion with radii $a=1.7$–$1.8$ Å inside the 4a-site cage in particular is expected to show the rattling motion over the off-center positions being away from the center of the cage. Actually, neutron scattering on $Pr_3Pd_{20}Ge_6$ and $Nd_3Pd_{20}Ge_6$ revealed sharp transition peaks, indicating a stable CEF splitting at the 8c site and no indication for CEF state at the 4a site.[8] These results may imply the obscure CEF state due to the off-center Ce ion at the 4a site contrary to the well-defined CEF splitting at the 8c site being a stable Ce ion position.

### F. $\Gamma_5$ rattling motion

A notable finding of Fig. 14 is that the ultrasonic dispersion in the $C_{44}$ mode associated with $\varepsilon_{xy}$-type strain indicates a rattling motion with a specific $\Gamma_5$ symmetry in $Ce_3Pd_{20}Ge_6$. It is expected that the Ce ion in the 4a cage with cubic symmetry $O_h$ favors off-center positions along one of the three principal directions of [100], [110], and [111]. As one can see, the cage at the 4a site in Fig. 1 is of particular interest in that no atom exists along the three fold [111] directions, while the Ge atom occupies the fourfold [100] directions and the Pd atom along the twofold [110] directions. This crystallographic character may promise a flat potential along the threefold [111] directions and profound potentials along the fourfold [100] and twofold [110] directions. Presumably the Ce ion at the 4a site prefers the off-center eight positions along the [111] directions, which are defined as $r_1=(a,a,a)$, $r_2=(-a,-a,a)$, $r_3=(-a,a,-a)$, $r_4=(a,-a,-a)$, $r_5=(a,a,-a)$, $r_6=(-a,-a,-a)$, $r_7=(a,-a,a)$, and $r_8=(-a,a,a)$. The atomic densities $\rho_i=\rho_i(r_i)(i=1$–$8)$ at the eight off-center positions are also defined. When 48 symmetry operators of the $O_h$ point group act on the atomic densities $\rho_i$, one can derive the transfer representation matrices with $8\times 8$ elements. Consequently, one obtains the characters $\chi_{rat}^{[111]}$ for the rattling motion by tracing the diagonal elements of the representation matrices. Using the characters $\chi_{rat}^{[111]}$ and the character table for the irreducible representations of $O_h$,[30] the rattling motion over the eight off-center positions along the [111] direction is reduced to the direct sum of $\Gamma_1(1D)\oplus\Gamma_2(1D)\oplus\Gamma_4(3D)\oplus\Gamma_5(3D)$.

Employing projection operators on appropriate atomic density $\rho_i$, we obtain the rattling modes for the irreducible representations as listed in Table I together with the elastic strains $\varepsilon_{\Gamma\gamma}$. One can see the presence of the $\Gamma_5$ rattling mode $\rho_{\Gamma 5,yz}, \rho_{\Gamma 5,zx}$, and $\rho_{\Gamma 5,xy}$ coupled to the strains $\varepsilon_{yz}$, $\varepsilon_{zx}$, and $\varepsilon_{xy}$, contrary to the absence of the $\Gamma_3$ rattling mode coupled to the strain $\varepsilon_u$, $\varepsilon_v$. This is consistent with the fact that the ultrasonic dispersion reveals in $C_{44}$ and is absent in $(C_{11}-C_{12})/2$. The Ce atom in the cage of $Ce_3Pd_{20}Ge_6$ obeys a harmonic oscillation of $\zeta(z)=(1/\pi z_0)1/2\exp(-z^2/2z_0^2)$ with a mean square displacement $z_0=(1/2\pi)(h\tau_0/M)^{1/2}$. The attempt time $\tau_0=3.1\times 10^{-11}$ sec and the mass $M=140m_p$ where $m_p$ is a proton mass, leads to the mean square displacement $z_0$ being approximately twice of off-center distances $a$ as $z_0=2a=0.48$ Å.[31]

The full symmetry $\Gamma_1$ rattling mode $\rho_{\Gamma 1}=\rho_1+\rho_2+\rho_3+\rho_4+\rho_5+\rho_6+\rho_7+\rho_8$ means a uniform atomic distribution with a fraction 1/8 at each of eight off-center positions. While the $\Gamma_5$ rattling mode, for instance $\rho_{\Gamma 5,xy}=\rho_1+\rho_2-\rho_3-\rho_4+\rho_5+\rho_6-\rho_7-\rho_8$, represents the anisotropic atomic distribution being quadrupole $O_{xy}$ at the lowest order such as fraction 1/4 at $r_1$, $r_2$, $r_5$, and $r_6$ and zero at $r_3$, $r_4$, $r_7$, and $r_8$, as shown in Fig. 15. The present group theoretical analysis for the rattling mode is essentially the same treatment previously argued for the charge fluctuation mode.[24,26,32] In the present system $Ce_3Pd_{20}Ge_6$, the thermally activated $\Gamma_5$ rattling mode may be a ground state and $\Gamma_1$, $\Gamma_2$, and $\Gamma_4$ may be excited states.

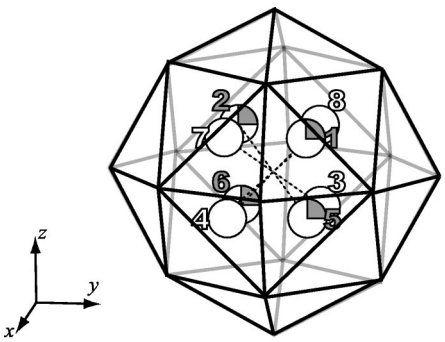


$$\rho_{\Gamma 5,xy}=\rho_1+\rho_2-\rho_3-\rho_4+\rho_5+\rho_6-\rho_7-\rho_8$$

FIG. 15. Schematic view for the $\Gamma_5$ rattling mode $\rho_{\Gamma 5,xy}$ due to the off-center Ce ion along the three-fold [111] direction in the 4a-site cage. The $\rho_{\Gamma 5,xy}$ represents that fractional atomic density 1/4 is located at $r_1$, $r_2$, $r_5$, and $r_6$ and null at $r_3$, $r_4$, $r_7$, and $r_8$. The freezing of the thermally activated motion of the $\Gamma_5$ rattling mode brings about the atomic tunneling state at low temperatures.

Our group recently found a similar ultrasonic dispersion around 30 K in a heavy fermion superconductor $PrOs_4Sb_{12}$ with a filled skutterudite structure. It should be noted that ultrasonic dispersion in the $(C_{11}-C_{12})/2$ mode of $PrOs_4Sb_{12}$ indicates a $\Gamma_3$ rattling motion of a Pr atom over six fractionally occupied positions along [100]. The dispersion of $(C_{11}-C_{12})/2$ in $PrOs_4Sb_{12}$ is contrary to the one of $C_{44}$ in the present compound of $Ce_3Pd_{20}Ge_6$.[14] The attempted time $\tau_0=8.8\times10^{-11}$ sec, activation energy $E=168$ K, and mean square displacement $z_0=0.80$ Å in $PrOs_4Sb_{12}$ are comparable to the present results of $Ce_3Pd_{20}Ge_6$.

The thermally activated $\Gamma_5$ rattling motion with fractional atomic state in $Ce_3Pd_{20}Ge_6$ dies out with decreasing temperature. At further low temperatures, the off-center tunneling state of Ce ions in the 4a-site cages will appear, which means a quantum state being occupying four positions, for instance at $r_1$, $r_2$, $r_5$, and $r_6$ for the case of $\rho_{\Gamma 5,xy}$, at the same time. The charge glass state in the inhomogeneous mixed valence compound $Sm_3Te_4$ revealed a low-temperature softening in elastic constants proportional to $\ln T$ resembles a structural glass.[26] The present scenario of the atomic tunneling of Ce ions in 4a-site cages in $Ce_3Pd_{20}Ge_6$ is also expected to show an elastic softening at low temperatures. However, the low-temperature quadrupole and magnetic orderings in $Ce_3Pd_{20}Ge_6$ may mask the character of the tunneling state in the present case. In order to clarify the tunneling and rattling in the present clathrate compounds, a low-temperature thermodynamic and ultrasonic measurements on $La_3Pd_{20}Ge_6$, without 4f-electron in particular, is required.

## IV. CONCLUDING REMARKS

In the present paper we have measured the elastic constants and thermal expansion of $Ce_3Pd_{20}Ge_6$. The characteristic elastic softening in $(C_{11}-C_{12})/2$ and $C_{44}$ is well described in terms of the quadrupole susceptibility for the $\Gamma_8$ ground state. The important finding is that $(C_{11}-C_{12})/2$ shows the huge softening of 50% towards $T_{Q1}=1.25$ K, and that $C_{44}$ exhibits a softening of 2.5% only. This result strongly indicates a FQ ordering with an order parameter of the $\Gamma_3$ symmetry in phase II below $T_{Q1}$. Actually we have successfully observed the sharp increase of $\Delta L/L=1.9\times10^{-4}$ in length along the [001] direction below $T_{Q1}$. This is evidence of $O_2^0$-type FQ ordering accompanied by the structural change from cubic lattice to tetragonal one at $T_{Q1}$ in $Ce_3Pd_{20}Ge_6$.

For the investigation of the magnetic phase diagram concerning the FQ phase II and the AFM phase III in $Ce_3Pd_{20}Ge_6$, elastic constants and thermal expansion in fields have been measured. We have found that the boundary from the paramagnetic phase I to the FQ phase II of $O_2^0$ shifts to higher temperatures with increasing magnetic fields. The result that the I-II phase transition becomes obscure in fields is similar to the liquid-gas transition approaching the critical end point under pressure. This result is consistent with the fact that the FQ order parameter $O_2^0$ in $Ce_3Pd_{20}Ge_6$ has a total symmetry under fields along the [001] direction.[5] The boundary from phase II to the AFM ordering shifts to lower temperatures, similar to the conventional AFM ordering.

We have found an ultrasonic dispersion in the $C_{44}$ mode, indicating a rattling motion with $\Gamma_5$ symmetry. Taking into account the absence of the atom along the [111] direction in the 4a-site cage, we have successfully picked up the specific $\Gamma_5$ rattling modes $\rho_{\Gamma 5,yz}$, $\rho_{\Gamma 5,zx}$, and $\rho_{\Gamma 5,xy}$ with a fractional atomic density over the eight minimum positions of potential along the fourfold [111], $[\bar{1}11]$, $[1\bar{1}1]$, and $[11\bar{1}]$ directions. The dispersion of the $C_{44}$ mode obeying the Debye formula revealed the thermally activated-type relaxation time of $\tau=\tau_0\exp(E/k_BT)$ for the $\Gamma_5$ rattling mode with an attempt time $\tau_0=3.1\times10^{-11}$ sec and an activation energy $E=70$ K. The estimated mean square displacement $z_0=0.48$ Å for the harmonic oscillation of the Ce atom leads to the distance of the potential minima along the [111] direction as $a=z_0/2=0.24$ Å. In order to confirm the anisotropic atomic distribution in the 4a-site cage, neutron or x-ray scattering is required. The freezing of the thermally activated motion due to the $\Gamma_5$ rattling mode with lowering temperature brings about the atomic tunneling state. By analogy of the charge glass compound $Sm_3Te_4$, Ce-ion tunneling is expected at low temperatures. The ultrasonic investigation on $La_3Pd_{20}Ge_6$ free from the long-range ordering due to 4f-electrons is now in progress to shed light on the tunneling and rattling in cages.

## ACKNOWLEDGMENT

This work was supported by a Grant-In-Aid for Scientific Research from the Ministry of Education, Culture, Sports, Science and Technology of Japan.

[1] D. Schmitt, P. Morin, and J. Pierre, J. Magn. Magn. Mater. **8**, 249 (1978).
[2] R. Takke, N. Dolezal, W. Assmus, and B. Lüthi, J. Magn. Magn. Mater. **23**, 247 (1981).
[3] H. Nakao, K. Magishi, Y. Wakabayashi, Y. Murakami, K. Koyama, K. Hirota, Y. Endoh, and S. Kunii, J. Phys. Soc. Jpn. **70**, 1857 (2001).
[4] S. Nakamura, T. Goto, S. Kunii, K. Iwashita, and A. Tamaki, J. Phys. Soc. Jpn. **63**, 623 (1994).
[5] R. Shiina, H. Shiba, and P. Thalmeier, Phys. Soc. Jpn. **66**, 1741 (1997); R. Shiina, O. Sakai, H. Shiba, and P. Thalmeier, *ibid.* **67**, 941 (1998).
[6] J. Kitagawa, N. Takeda, and M. Ishikawa, Phys. Rev. B **53**, 5101 (1996).
[7] A. V. Grivanov, Yu. D. Seropegin, and O. I. Bodak, J. Alloys Compd. **204**, L9 (1994).
[8] L. Keller, A. Dönni, M. Zolliker, and T. Komatsubara, Physica B **259-261**, 336 (1999).
[9] J. Kitagawa, N. Takeda, M. Ishikawa, T. Yoshida, A. Ishiguro, N. Kimura, and T. Komatsubara, Phys. Rev. B **57**, 7450 (1998).
[10] O. Suzuki, T. Horino, Y. Nemoto, T. Goto, A. Dönni, T. Komatsubara, and M. Ishikawa, Physica B **259-261**, 334 (1999); T. Goto, T. Horino, Y. Nemoto, T. Yamaguchi, A. Dönni, O. Suzuki, and T. Komatsubara, *ibid.* **312-313**, 492 (2002).
[11] A. Dönni, T. Herrmannsdörfer, P. Fischer, L. Keller, F. Fauth, K. A. McEwen, T. Goto, and T. Komatsubara, J. Phys.: Condens. Matter **12**, 9441 (2000).
[12] L. Mihaly, Nature (London) **395**, 839 (1998); V. Keppens, D. Mandrus, B. C. Sales, B. C. Chakoumakos, P. Dai, R. Coldea, M. B. Maple, D. A. Gajewski, E. J. Freeman, and S. Bennington, *ibid.* **395**, 876 (1998).
[13] V. Keppens, B. C. Sales, D. Mandrus, B. C. Chakoumakos, and C. Laermans, Philos. Mag. Lett. **80**, 807 (2000).
[14] T. Goto, Y. Nemoto, K. Sakai, T. Yamaguchi, M. Akatsu, T. Yanagisawa, H. Hazama, K. Onuki, H. Sugawara, and H. Sato (unpublished).
[15] E. Kanda, T. Goto, H. Yamada, S. Suto, S. Tanaka, T. Fujita, and T. Fujimura, J. Phys. Soc. Jpn. **54**, 175 (1985); H. Yamada, S. Tanaka, Y. Kayanuma, and T. Kojima, *ibid.* **54**, 1180 (1985).
[16] P. Thalmeier and B. Lüthi, in *Handbook on the Physics and Chemistry of Rare Earths*, edited by K. A. Gschneider, Jr. and L. Eyring (North-Holland, Amsterdam, 1991), Vol. 14. Chap. 96.
[17] T. Goto, Y. Nemoto, Y. Nakano, S. Nakamura, T. Kajitani, and S. Kunii, Physica B **281-282**, 586 (2000); T. Yamaguchi, M. Akatsu, Y. Nakano, T. Washizawa, Y. Nemoto, T. Goto, A. Dönni, S. Nakamura, and S. Kunii, *ibid.* **329-333**, 622 (2003).
[18] A. Dönni, L. Keller, P. Fischer, Y. Aoki, H. Sato, F. Fauth, M. Zolliker, T. Komatsubara, and Y. Endoh, J. Phys.: Condens. Matter **10**, 7219 (1998); N. Kimura, N. Tateiwa, M. Nakayama, H. Aoki, T. Komatsubara, T. Sakon, M. Motokawa, Y. Koike, and N. Metoki, Physica B **259-261**, 338 (1999).
[19] T. Herrmannsdörfer, A. Dönni, P. Fischer, L. Keller, E. Clementyev, A. Furrer, S. Mango, B. van den Brandt, and H. Kitazawa, J. Alloys Compd. **323-324**, 509 (2001).
[20] T. Herrmannsdörfer, A. Dönni, P. Fischer, L. Keller, G. Böttger, M. Gutmann, H. Kitazawa, and J. Tang, J. Phys.: Condens. Matter **11**, 2929 (1999).
[21] T. Herrmannsdörfer, A. Dönni, P. Fischer, L. Keller, and H. Kitazawa, Physica B **281-282**, 167 (2000).
[22] O. Suzuki, T. Goto, S. Nakamura, T. Matsumura, and S. Kunii, J. Phys. Soc. Jpn. **67**, 4243 (1998); M. Akatsu, T. Goto, Y. Nemoto, O. Suzuki, S. Nakamura, and S. Kunii, *ibid.* **72**, 205 (2003).
[23] Y. Nemoto, H. Aoki, T. Goto, A. Ochiai, and T. Suzuki, Physica B **259-261**, 275 (1999).
[24] T. Goto and B. Lüthi, Adv. Phys. **52**, 67 (2003).
[25] A. Tamaki, T. Goto, S. Kunii, T. Suzuki, T. Fujimura, and T. Kasuya, J. Phys. C **18**, 5849 (1985).
[26] Y. Nemoto, T. Goto, A. Ochiai, and T. Suzuki, Phys. Rev. B **61**, 12 050 (2000).
[27] P. W. Anderson, B. I. Halperin, and C. M. Varma, Philos. Mag. **25**, 1 (1972).
[28] See, for example, S. Hunklinger and W. Arnold, *Physical Acoustics* (Academic, New York, 1976), Vol. XII, p. 155.
[29] See, for example, *Amorphous Solids: Low-Temperature Properties*, edited by W. A. Phillips (Springer, Berlin, 1981).
[30] T. Inui, Y. Tanabe, and Y. Onodera, *Group Theory and Its Applications in Physics* (Springer, Berlin, 1990).
[31] D.L. Cox and A. Zawadowski, Adv. Phys. **47**, 599 (1998).
[32] T. Goto, Y. Nemoto, A. Ochiai, and T. Suzuki, Phys. Rev. B **59**, 269 (1999).